Eur. Phys. J. Spec. Top.
https://doi.org/10.1140/epjs/s11734-021-00225-7

THE EUROPEAN PHYSICAL JOURNAL SPECIAL TOPICS

Regular Article

Eisenbud–Wigner–Smith time delay in atom–laser interactions

P. C. Deshmukh[1,2,a], S. Banerjee[3,4,b], A. Mandal[5,c], and S. T. Manson[6,d]

[1] Department of Physics and CAMOST, Indian Institute of Technology Tirupati, Tirupati, India
[2] Department of Physics, Dayananda Sagar University, Bengaluru 560114, India
[3] Department of Physics, IIT Madras, Chennai 600036, India
[4] TCG Centres for Research and Education in Science and Technology, Kolkata 700016, India
[5] Department of Physical Sciences, Indian Institute of Science Education and Research Mohali, Mohali 140306, India
[6] Department of Physics and Astronomy, Georgia State University, Atlanta, GA 30303, USA

Received 7 April 2021 / Accepted 13 July 2021
© The Author(s), under exclusive licence to EDP Sciences, Springer-Verlag GmbH Germany, part of Springer Nature 2021

Abstract Recent development of ultrafast measurement technique on the sub-femtosecond time scale has enabled us to see the atom–laser interaction in real time. One of the important observable to study the temporally resolved dynamics is the various time delay in the process. Time delay is an experimentally measurable quantity, where the time is not. Time delay in quantum collisions and in photoionization/photodetachment of atomic and molecular systems is reviewed. Formalism of time delay in the context of quantum collision by Eisenbud and Wigner that by Smith and their equivalence is discussed. The time-reversal symmetry between solutions with outgoing and ingoing wave boundary conditions allow us to interpret photoionization/photodetachment as half-scattering. Subsequently, the formalism of Eisenbud–Wigner–Smith time delay is extended in photoionization/photodetachment from collision. We discuss that the time delay can be written as a self-adjoint quantum operator which depicts its measurability. On the experimental side, the measurement protocols are reviewed for attosecond streaking and RABBITT. Along with the EWS time delay, the measurement introduces an additional (which is negative) time delay. From the measurement of total delay and an analytical/numerical estimate of the measurement induced part, one gets the EWS time delay in the process. A few illustrative examples of studies on time delay are given to get a flavour of the outstanding advances made in this field in the last 2 decades.

Introduction

Advancements in ultrafast laser technology have opened up exciting opportunities to investigate electron dynamics within atoms and molecules on their natural time scale. Photoionization was considered to be an instantaneous process, since Einstein's explanation of the photoelectric effect for about a hundred years until few experiments [1–3] recently revealed tiny time delay, of the order of attoseconds, in the process. Theoretical description of time delay was however provided nearly 7 decades ago, by Eisenbud [4] and Wigner [5] in the context of quantum scattering. Soon thereafter, an equivalent formalism of scattering time delay was provided by Smith [6]. A large number of articles on time delay, for example, [7–26], in the last 2 decades show the increased attention this topic has received, primarily because of the laboratory possibilities to measure such a short delay using sophisticated experimental techniques. Time is considered only as a parameter in quantum mechanics; no operator represents it. Time and energy constitute a classical canonically conjugate pair and there also exists a quantum uncertainty relation involving them, similar to that for position and momentum; but there is a fundamental difference. Position and momentum are represented by self-adjoint operators in quantum mechanics, and they correspond to physically measurable parameters. There is no Hermitian operator in quantum mechanics for time; it is not a measurable quantity. Its canonically conjugate parameter is energy. As is very well known, energy is represented by the Hamiltonian, which is Hermitian. Time delay in a scattering phenomenon can however be measured. It can be represented by a Hermitian operator. Time delay, on the contrary, can in fact be measured, and can therefore be represented by a Hermitian operator. This article is organized in three sections. In the first section, the theoretical development of time delay is discussed. The Eisenbud–Wigner and Smith formalism is reviewed in this section. Also, we point out how this approach is applicable not merely to analyse time delay in quan-

[a] e-mail: pcd@iittp.ac.in
[b] e-mail: souravbanrj444@gmail.com
[c] e-mail: ankur@iisermohali.ac.in (corresponding author)
[d] e-mail: smanson@gsu.edu

SPI Journal: 11734 MS: 0225 ☐ TYPESET ☐ DISK ☐ LE ☐ CP Disp.:2021/7/19 Pages: 14 Layout: EPJST

tum collisions, but also in atomic photoionization. Also, in this section, the Hermitian operator associated with time delay is discussed. The first section would follow the more elaborate treatment we dealt with in Reference [27], but somewhat briefly. The second section describes various experimental techniques developed in recent years to measure time delay. In the third section, we review some interesting studies on time delay in photoionization from atoms, molecules, and solid surfaces.

1 The notion, and measurability, of time delay

When an incident projectile interacts with a potential, its wavefunction experiences a phase shift [28] which embodies all physical information about the interaction potential. The incoming projectile beam is never strictly monoenergetic; it is represented by a wavepacket

$$\Phi_{\mathbf{b},l}(\mathbf{r},t) = \frac{1}{(2\pi)^{3/2}} \iiint d^3\mathbf{k} \times \left[A_l(\mathbf{k}) e^{+i\{\mathbf{k}\cdot(\mathbf{r}-\mathbf{b})-\omega(\mathbf{k})t\}} \right]. \quad (1)$$

The symbols and notation we employ are essentially those from Reference [27]. In the above equation, b is the impact parameter, and the lth partial wave is indicated by the subscript l. The solution to the scattering problem, represented by a superscript '+' to indicate outgoing wave boundary conditions, is expressed as [27,28]

$$\Psi^{+}_{\mathbf{b},l}(\mathbf{r},t) \underset{r\to\infty}{\longrightarrow} \Phi_{\mathbf{b},l}(\mathbf{r},t) + \frac{1}{(2\pi)^{3/2}} \iiint d^3\mathbf{k} \times \left[A_l(\mathbf{k}) e^{-i\mathbf{k}\cdot\mathbf{b}} f_l\left(\mathbf{k},\hat{\Omega}\right) \frac{e^{i(kr-\omega(\mathbf{k})t)}}{r} \right]. \quad (2)$$

The phase corresponding to each momentum component in the scattered wavepacket is

$$\xi_l(\mathbf{k}) = kr - \omega(\mathbf{k})t + \alpha(\mathbf{k}) + \Lambda_l(\mathbf{k},\hat{\Omega}) - \mathbf{k}\cdot\mathbf{b}, \quad (3)$$

where $\Lambda_l(\mathbf{k},\hat{\Omega})$ is the phase of the complex scattering amplitude $f_l\left(\mathbf{k},\hat{\Omega}\right)$, ($|f_l\left(\mathbf{k},\hat{\Omega}\right)|$ being its magnitude), and $\alpha(\mathbf{k})$ is the phase of the complex amplitude $A_l(\mathbf{k})$ ($|A_l(\mathbf{k})|$ being its magnitude). Random changes in the phase ξ_l would cause the integration in the momentum space [in Eq. (2)] to vanish. We shall therefore be interested in wave packets for which the phase waves ξ_l do not change much with momentum, around some particular value $\mathbf{k}_0$. The condition for stationary phase is

$$[\boldsymbol{\nabla}_k \xi_l(\mathbf{k})]_{\mathbf{k}=\mathbf{k}_0} = \mathbf{0}, \quad (4)$$

which is satisfied when

$$r\hat{k}_0 - \mathbf{v}_g t - \mathbf{r}_0 + \boldsymbol{\rho}_l(\hat{\Omega}) - \mathbf{b} = \mathbf{0}, \quad (5)$$

where

$$\boldsymbol{\rho}_l(\hat{\Omega}) = [\boldsymbol{\nabla}_k \Lambda_l(\mathbf{k})]_{\mathbf{k}=\mathbf{k}_0}, \quad (6a)$$

$$\mathbf{v}_g = [\boldsymbol{\nabla}_k \omega(\mathbf{k})]_{\mathbf{k}=\mathbf{k}_0}, \quad (6b)$$

$$\text{and } \mathbf{r}_0 = -[\boldsymbol{\nabla}_k \alpha(\mathbf{k})]_{\mathbf{k}=\mathbf{k}_0}. \quad (6c)$$

The instantaneous position of the centre of the wavepacket propagation along the direction $\mathbf{k}_0$ then is

$$r(t) = v_g t + \left(\mathbf{r}_0\cdot\hat{k}_0\right) + \left(\mathbf{b}\cdot\hat{k}_0\right) - \left(\boldsymbol{\rho}_l\cdot\hat{k}_0\right) = v_g t + r_0 k_0 - \left(\boldsymbol{\rho}_l\cdot\hat{k}_0\right). \quad (7)$$

The peak of the wavepacket is spatially shifted by amount $\left(\boldsymbol{\rho}_l\cdot\hat{k}_0\right)$ relative to a wavepacket that does not encounter the scattering potential. The time delay corresponding to this spatial shift is the Eisenbud–Wigner time delay

$$\tau_{WE} = \frac{\boldsymbol{\rho}_l(\hat{\Omega})\cdot\hat{k}_0}{v_g} = \frac{\frac{\mathrm{d}\Lambda_l}{\mathrm{d}k}\big|_{k=k_0}}{\frac{\mathrm{d}\omega}{\mathrm{d}k}\big|_{k=k_0}} = \left.\frac{\mathrm{d}\Lambda_l}{\mathrm{d}\omega}\right|_{k=k_0} = \hbar\left.\frac{\mathrm{d}\Lambda_l}{\mathrm{d}E}\right|_{E=E_0} = \hbar\left.\frac{\mathrm{d}}{\mathrm{d}E}\left[\arg f_l(\mathbf{k},\hat{\Omega})\right]\right|_{E=E_0}. \quad (8a)$$

It is well known that the scattered part involves an extra phase shift of $2\delta_l(k)$ due to the interaction with the potential. Half of the total phase shift, ti.e., $\delta_l(k)$ occurs when the projectile enters the scattering zone, and the other half occurs when the projectile recedes from it. Therefore, the time delay in the lth partial wave is

$$\tau^{(l)}_{WE} = 2\hbar\frac{\mathrm{d}\delta_l}{\mathrm{d}E}. \quad (8b)$$

Smith [6,29] interpreted time delay in quantum scattering in terms of the ratio of the excess number of particles in the scattering region at an instant of time to the rate of flow of the projectiles through that region. The scattering time delay is therefore

$$\tau_{Smith} = \frac{\text{Excess number of particles near scattering centre}}{\text{Ingoing (or Outgoing flux)}}. \quad (9)$$

We consider scattering due to a spherically symmetric potential $V(r)$. The general solution to the Schrödinger equation in the spherical polar coordinate system is

$$\psi_l(\mathbf{r},t) = exp(-iEt/\hbar)R_l(r)Y_l^m(\hat{r}) = exp(-i\omega t)R_l(r)Y_l^m(\hat{r}), \quad (10)$$

SPI Journal: 11734 MS: 0225 ☐ TYPESET ☐ DISK ☐ LE ☐ CP Disp.:2021/7/19 Pages: 14 Layout: EPJST

Author Proof

where R_l represents the radial wavefunction, Y_l^m stands for the spherical harmonics, and the factor $e^{-i\omega t}$ denotes the dynamic phase of the stationary quantum state. We discuss the radial solutions in terms of $u_l(r) = rR_l(r)$.

The solution to the radial wavefunction is obtained by substituting $R_l = \frac{u_l}{r}$ to the radial differential equation. The simplest example, for the partial wave with $l = 0$ in the absence of any potential, is

$$\left\{u^+_{l=0}(r), u^-_{l=0}(r)\right\}_{V=0} = \{exp(+ikr), exp(-ikr)\}. \tag{11}$$

The general solution corresponding to the l^{th} partial wave is a superposition of the base pair $\left\{u_l^+(r), u_l^-(r)\right\}$ which can be obtained from $\left\{u^+_{l=0}(r), u^-_{l=0}(r)\right\}$ using a recursion relation.

We shall employ the base pair $\left\{u_l^+(r), u_l^-(r)\right\}$ comprising of components corresponding to a wave moving outward from the scattering centre (i.e., r increases with t for $u_l^+(r)$) and those moving toward the centre (i.e., r decreases with t for $u_l^-(r)$). Thus, the scattering components may be expressed as

$$\varphi_{\text{in},l} = Cu_l^-(r), \tag{12a}$$

and

$$\varphi_{\text{out},l} = Ce^{2i\delta_l(k)}u_l^-(r), \tag{12b}$$

where C is the normalization constant, and $\varphi_{\text{in},l}$ and $\varphi_{\text{out},l}$, respectively, represent the radial ingoing and the outgoing wave functions.

The asymptotic radial solutions are then represented as

$$u_l(r \to \infty) = C\left[u_l^-(r) - e^{2i\delta_l}u_l^+(r)\right]. \tag{13}$$

Determination of the numerator in Eq. (9) requires the excess density in the scattering region compared to that in the absence of any potential, ti.e., $V = 0$. The excess density over a range R from the centre is

$$D_{l,\text{excess}}(R) = \iiint_{r\le R} \left[\rho_{l,V\neq 0} - \rho_{l,V=0}\right] d\zeta, \tag{14}$$

where $\rho_l = \psi_l * (\mathbf{r})\psi_l(\mathbf{r})$ is the probability density, and $d\zeta = r^2 dr sin\theta d\theta d\varphi = r^2 dr d\omega$ is the integration volume element. To determine the denominator of Eq. (9), we note that it is a measure of the ingoing flux, or the outgoing flux; both being the same on account of the fact that the current density vector $\mathbf{j}(\mathbf{r})$ is solenoidal. Now, the ingoing flux is

$$F_{\text{in}} = \oiint \mathbf{j}_{\text{in}} \cdot \mathbf{ds} = \frac{\hbar}{2mi}\left[\frac{\varphi^*_{\text{in},l}\frac{\partial\varphi_{\text{in},l}}{\partial r} - \varphi_{\text{in},l}\frac{\partial\varphi^*_{\text{in},l}}{\partial r}}{r^2}r^2\right]_{r=R}$$
$$\oiint d\omega Y_l^{m*}Y_l^m = -CC^*v = -F_{\text{out}}. \tag{15}$$

Normalization with unit incident flux gives

$$C = v^{-1/2}, \tag{16}$$

where $v = \hbar k/m$.

In the absence of any potential, (ti.e., when $V = 0$), $\delta_l = 0$, and the probability density is given by

$$\rho_{l,V=0} = \psi^*_{l,V=0}(\mathbf{r})\psi_{l,V=0}(\mathbf{r}) = \frac{2CC^*}{r^2}Y_l^{m*}Y_l^m. \tag{17}$$

Following Smith [6], and as worked out some details in Ref. [27], it follows from Eq. (9) that the excess density (Eq. (14)) is given by:

$$\begin{aligned} D_{l,\text{excess}}(R\to\infty) &= \lim_{R\to\infty}\left\{\iiint_{r\le R}\left[\rho_{l,V\neq 0} - \rho_{l,V=0}\right]d\zeta\right\} \\ &= \lim_{R\to\infty}\left[2\hbar\frac{\partial\delta_l}{\partial E} + \frac{2R}{v} - \frac{\hbar}{2E}sin\left(2kR + 2\delta_l - \frac{l\pi}{2}\right)\right. \\ &\quad \left. + \frac{G_l}{R} - \frac{2R}{v}\right]. \end{aligned} \tag{18}$$

Cancellation of oscillatory term in the above expression that would result from integration over different r and k gives

$$\tau_{\text{Smith}} = 2\hbar\frac{\partial\delta_l}{\partial E} = \tau_{\text{WE}}. \tag{19}$$

We shall therefore denote scattering time delay as τ_{EWS}, the subscript EWS (also called Wigner or WES) highlighting the equivalence between the Eisenbud-Wigner's and Smith's formulation.

Recognizing that time itself is not an observable, and therefore not representable by a Hermitian operator [29], we now ask if time *delay*, if not time itself, is observable. This would require the representation of time delay by a self-adjoint operator. Following the treatment in References [30,31], we now demonstrate that this requirement is indeed satisfied. We compare free (unscattered) states φ with scattered states ψ. We consider their time evolution under a unitary time evolution operators, U. The time evolution operator involves the Hamiltonian, and it is therefore different for free states and for wave functions scattered by a potential.

Accordingly

$$\varphi_t = U_t^{V=0}\varphi_{t=0}, \text{ where } U_t^{V=0} = e^{-\frac{iHt}{\hbar}}\Big|_{H=T}, \tag{20a}$$

and

$$\psi_t = U_t^{V\neq 0}\psi_{t=0}, \text{ where } U_t^{V\neq 0} = e^{-\frac{iHt}{\hbar}}\Big|_{H=T+V}. \tag{20b}$$

Author Proof

Author Proof

In Eqs. (20a) and (20b), the subscript $H = T$ represents the free-particle Hamiltonian consisting of the kinetic energy operator T alone, and $H = T+V$ represents the Hamiltonian inclusive of a non-zero scattering potential. We consider the scattering interaction to take place at $t = 0$ (Fig. 1). Much before this event ($t \to -\infty$), and much later $t \to +\infty$, the particle would be so far away from the scattering zone that the particle would be free from any interacting potential. The states φ and ψ are therefore indistinguishable from each other in the limit $t \to \pm\infty$. We consider two asymptotic free states, φ_{in} and φ_{out}, which resemble states for $t \to -\infty$ and $t \to +\infty$, respectively. This scenario is expressed by the following relations:

$$\lim_{t\to-\infty} \left\| U_t^{V\neq0}\psi_{t=0} - U_t^{V=0}\varphi_{\text{in},t=0} \right\|, \tag{21a}$$

ti.e.

$$\psi_{t=0} = lim_{t\to-\infty} U_t^{V\neq0\dagger} U_t^{V=0}\varphi_{\text{in},t=0}, \tag{21b}$$

and

$$\lim_{t\to+\infty} \left\| U_t^{V\neq0}\psi_{t=0} - U_t^{V=0}\varphi_{\text{out},t=0} \right\|, \tag{21c}$$

ti.e.,

$$\psi_{t=0} = lim_{t\to+\infty} U_t^{V\neq0\dagger} U_t^{V=0}\varphi_{\text{out},t=0}. \tag{21d}$$

Using Møller operators, defined as

$$\Omega_{\pm} = lim_{t\to\pm\infty} U_t^{V\neq0\dagger} U_t^{V=0}, \tag{22a}$$

the expressions in Eq. (21) reduce to [30,31]

$$\Omega_-\varphi_{\text{in},t=0} = \psi_{t=0} = \Omega_+\varphi_{\text{out},t=0}, \tag{22b}$$

i.e.,

$$\varphi_{\text{out},t=0} = \Omega_+\Omega_-\varphi_{\text{in},t=0}. \tag{22c}$$

Now, the scattering operator S, by definition, produces state φ_{out} operating on φ_{in}, ti.e.

$$\varphi_{\text{out},t=0} = S\varphi_{\text{in},t=0}, \tag{23a}$$

with

$$S = \Omega_+^{\dagger}\Omega_-. \tag{23b}$$

We now proceed to construct a Hermitian operator for time delay. The self-adjoint property of this operator is an essential property that time delay must have if it is to represent a measurable physical quantity. We have

$$S(E) = e^{2i\delta(E)}, \tag{24a}$$

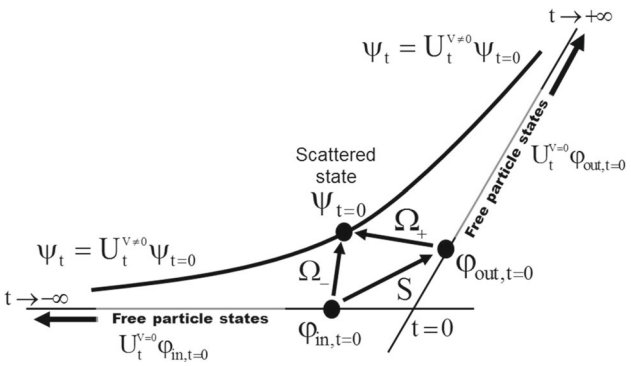

Fig. 1 Schematic diagram showing the scattering process. The Møller operators produce the scattering states and the scattering operator produces the scattered outgoing states from the incoming states, both considered in the asymptotic region

ti.e.

$$2\delta = \text{Im}\left[ln\left\{S(E)\right\}\right]. \tag{24b}$$

The Eisenbud–Wigner–Smith time delay is quantized as follows:

$$\begin{aligned}\tau_{\text{EWS}} \to \tau_{\text{EWS}}^{\text{Operator}} &= \hbar\frac{\partial}{\partial E}[2\delta]^{\text{Operator}} \\ &= \hbar\frac{\partial}{\partial E}\left[\text{Im}\left\{ln[S(E)]\right\}\right] = \hbar\text{Im}\frac{\partial}{\partial E}\left[ln[S(E)]\right],\end{aligned} \tag{25a}$$

ti.e.

$$\begin{aligned}\tau_{\text{EWS}}^{\text{Operator}} &= \text{Re}\left[-i\hbar\left\{S(E)\right\}^{-1}\frac{\partial}{\partial E}\left\{S(E)\right\}\right] \\ &= -i\hbar S(E)^{\dagger}S'(E),\end{aligned} \tag{25b}$$

where the prime denotes differentiation with respect to energy.

Now, differentiating $S(E)^{\dagger}S(E)$ with respect to energy gives

$$S'(E)^{\dagger}S(E) + S(E)^{\dagger}S'(E) = 0. \tag{26}$$

Therefore, from Eq. (25b), we have

$$\tau_{\text{EWS}}^{\text{Operator}} = +i\hbar S'(E)^{\dagger}S(E), \tag{27}$$

and

$$\left(\tau_{\text{EWS}}^{\text{Operator}}\right)^{\dagger} = \left[-i\hbar S(E)^{\dagger}S'(E)\right] = \left(\tau_{\text{EWS}}^{\text{Operator}}\right). \tag{28}$$

The hermiticity of the Eisenbud–Wigner–Smith time delay operator makes it appropriate to represent a measurable property, namely the time delay, even though

SPI Journal: 11734 MS: 0225 ☐ TYPESET ☐ DISK ☐ LE ☐ CP Disp.:2021/7/19 Pages: 14 Layout: EPJST

Author Proof

time itself is not measurable and hence not representable by a Hermitian operator. Hermiticity is an important property of the operatory associated with measurable observables and it is satisfying to note that time delay is representable by a Hermitian operator. However, in a complete theory, there are other mathematical considerations [32,33] involved in defining measurability. The treatment of scattering time delay is more general in the sense that it involves the Møller operators and the scattering operator. Detailed discussion on the operator formalism is available in Ref. [30,31] where the authors provide extensive mathematical treatment to arrive at the hermitian nature of the time-delay operator.

Time-reversal symmetry enables one to extend the EWS formalism of time delay in quantum collisions to the dynamical processes of photoionization of a neutral atom, and also photodetachment of a negative ion. This symmetry likens the incident plane wave in an electron–atom collision event to the wavefunction of the time-reversed process consisting of the escaping photoelectron in the photoionization of an atom, or photodetachment of a negative ion. Concurrently, the cancellation of all ingoing spherical waves in the scattered solution in electron–atom collisions corresponds to that of all outgoing waves in the initial state of photoionization/photodetachment. Accordingly, description of the electron–atom collision employs the *outgoing* wave boundary conditions, whereas that of photoionization/photodetachment employs *ingoing* wave boundary conditions. Since the escaping photoelectron does not even exist in the *initial* state of photoionization (photodetachment) which consists a neutral atom (negative ion) and a photon, this process is often called as *half-scattering*; the final states however being the same in electron–atom collision and atomic photoionization. We refer the readers to References [27,34,35] for a more detailed discussion on the connections between solution to the quantum collision dynamics as opposed to atomic photoionization. The relationships between these time-reversed processes are depicted in Figs. 2 and 3. As the discussion below will demonstrate, we shall appreciate why Wigner preferred the expression motion reversal [36] over time-reversal.

The solution for a collision with outgoing wave boundary conditions indicated by a superscript + is given in Eq. (29a)

$$\psi^{+}_{\rm Tot}(\mathbf{r},t)\big|_{r\to\infty}\, e^{+i(kz-\omega t)} + \frac{e^{+i(kr-\omega t)}}{r}\left\{\frac{1}{2ik}\sum_{l=0}^{\infty}(2l+1)[e^{2i\delta_l(k)}-1]P_l(cos\theta)\right\}. \tag{29a}$$

The time-reversed solution, with ingoing wave boundary conditions, for atomic photoionization (photodetachment), is indicated by a superscript −, and given in Eq. (29b)

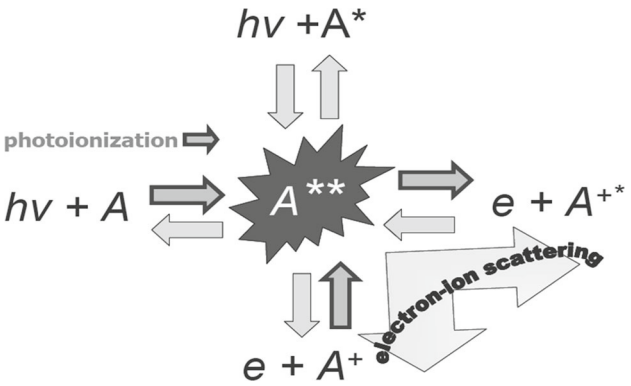

Fig. 2 Schematic diagram [34] showing that photoionization is *half* scattering

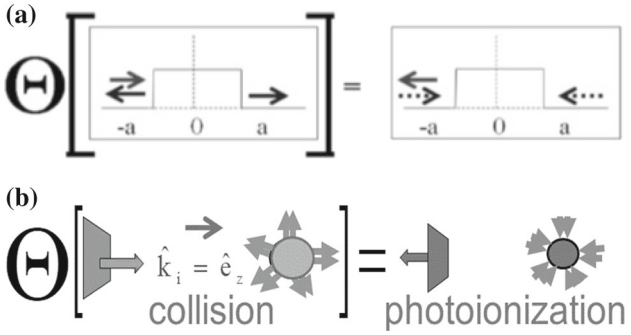

Fig. 3 **a** Schematic diagram depicting photoionization as half-scattering in a one-dimensional scenario. This figure demonstrates *motion reversal* that is referred to in the text. **b** Schematic diagram showing that the photoionization process is expressible as the time-reversal operator Θ operating on a quantum collision process

$$\psi^{-}_{\rm Tot}(\mathbf{r},t)\big|_{r\to\infty}\, e^{+i(kz+\omega t)} + \frac{e^{+i(kr+\omega t)}}{r}\left\{\frac{1}{2ik}\sum_{l=0}^{\infty}(2l+1)[e^{2i\delta_l(k)}-1]P_l(cos\theta)\right\}. \tag{29b}$$

These solutions are depicted in Fig. 3, in which Θ is the *anti-unitary* time-reversal operator [35].

The connection between electron–atom collisions and atomic photoionization enables the application of the EWS time delay formalism, which was developed originally in the context of quantum collision theory, also to atomic photoionization/photodetachment. This is remarkable, since photoionization was considered to be an instantaneous process for almost a century since Einstein's account of the photoelectric effect. Time delay in photoionization has now developed into a very active area of research, see, e.g., [2,3,37–54], to probe atomic dynamics on the natural time scale of electron dynamics in atoms. From Eqs. (29a) and (29b), which, respectively, correspond to collisions and atomic photoionization, we obtain the following connection:

$$\Theta\left[\psi^{+}_{\rm Tot}(\mathbf{r},t)\right] \underset{r\to\infty}{\longleftrightarrow} \left[\psi^{+}_{\rm Tot}(\mathbf{r},t)\right], \tag{30}$$

SPI Journal: 11734 MS: 0225 ☐ TYPESET ☐ DISK ☐ LE ☐ CP Disp.:2021/7/19 Pages: 14 Layout: EPJST

where Θ is the anti-unitary time-reversal (rather, motion reversal) operator.

As mentioned above, photoionization must be regarded as half-scattering. Hence, the factor '2' in Eq. (19) does not apply, and the photoionization time delay is given by

$$\tau_{\mathrm{EWS}}^{\mathrm{Photoionization}} = \hbar \frac{\partial \delta_l}{\mathrm{d}E} = \hbar \frac{\partial}{\partial E} \left[\arg \left\langle f \left| \hat{T} \right| i \right\rangle \right] \Big|_{E=E_0}, \tag{31}$$

where $\hat{T}$ represents the interaction operator responsible for the transition of the atom from the bound initial state $|i\rangle$ to the final continuum state $|f\rangle$. Time delay studies in the domain of photoionization/photodetachment are extremely valuable, since the results are very sensitive to electron correlations and relativistic effects which determine the phase of the complex transition matrix amplitude $\left\langle f \left| \hat{T} \right| i \right\rangle$ in Eq. (31). Accurate determination of this quantity requires very powerful and sophisticated theoretical methodologies [55–58]. Experimental determination of time delay is a daunting task; the advances made by experimentalists are, however, very impressive. In the next section, we overview some of the major advances made on the experimental front.

2 Measurement of EWS time delay in photoemission

Absolute EWS time delay has not been measured experimentally, since the group delay of the ionizing pulse with respect to the probe pulse is not measured. Thus, one performs relative EWS time delay measurements which cancels out the group delay of the pump pulses. To carry out an observation on the atomic time scale, one requires coherent ultrashort pulses in the near UV–XUV spectral range. This is achieved by generating high harmonics of an ultra-intense laser that employs the chirped pulse amplification technique [59], for which a share of the 2018 Nobel prize in physics was awarded. High harmonic generation (HHG) is well understood in terms of a three-step model [60,61]. A low-frequency, high-intensity laser field ejects an atomic electron through tunnelling in the first step. The photoelectron gains energy from the electric field of the laser light and is accelerated back toward the parent ion as the direction of the electric field reverses in the second step. This photoelectron can recombine with the ion, emitting a high energy photon in the third step. One can produce an attosecond pulse train (APT) or an isolated attosecond pulse (IAP) at relevant spectral domains using HHG. The IAP/APT is one of the main ingredients of attosecond scale pump-probe experiment. A schematic diagram of two HHG spectra is shown in Fig. 4c where the black curve represents the spectrum originating from a few tens of optical cycle monochromatic laser (typically in IR range) pulses interacting with atomic systems. A section of this spectrum can be used to produce an APT where the pulses are separated by half of the optical cycle (see Fig. 4a). Instead of discrete spectra, one can create a continuum of harmonics, as shown in dashed curve in Fig. 4c, by employing a few optical cycle pulses interacting with atoms or by means of some gating mechanism. In the time domain, the selected part of these continuum harmonics would give an IAP, as shown in Fig. 4b. Attosecond scale pump-probe measurement together with theoretical analysis gave rise the direct observation of attosecond photoemission phenomena from atoms, molecules, and condensed matter systems [2,3,63–68].

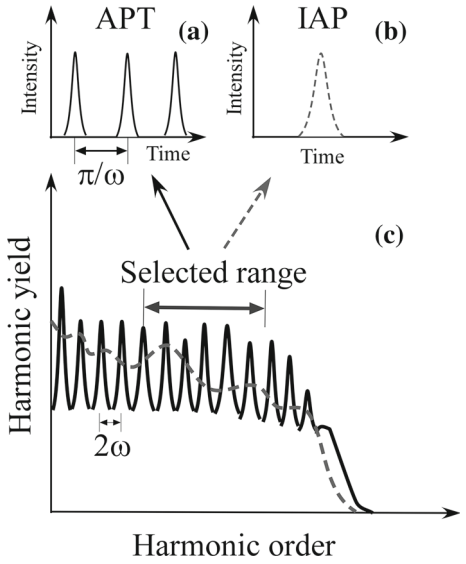

Fig. 4 Schematic diagram of APT, IAP from a selected portion of the high harmonic spectra marked as green arrow in **a**, **b**, and **c**, respectively

In the pump–probe technique, the total observed time delay can be written as

$$\tau_{\mathrm{atomic}} \cong \tau_{\mathrm{EWS}}^{\mathrm{photoionization}} + \tau_{\mathrm{measurement}}, \tag{32}$$

where τ_{atomic} is the total time delay measured in the experiment, $\tau_{\mathrm{EWS}}^{\mathrm{photoionization}}$ is the intrinsic time delay associated with the one photon (pump) transition [see Eq. (31)] and $\tau_{\mathrm{measurement}}$ is the delay induced by the measurement process (probe). A number of pump-probe tools are developed such as streaking, RABBITT, attoclock, attosecond transient absorption, *etc.* A schematic of attosecond streaking is shown in Fig. 5. This is based on XUV IAP pump which is ionizing the atoms and an IR probe which serves as a clock [2,62]. The IR field is applied with a controlled delay (τ) with respect to the ionizing XUV pulse, as shown in Fig. 5a. The final momentum of the photoelectron at the detector as a function of the delay τ is given by

$$\mathbf{p}_{\mathrm{final}}(\tau) = \mathbf{p}_{\mathrm{initial}} - \mathbf{A}_{\mathrm{IR}}(\tau + \tau_{\mathrm{Streaking}}), \tag{33}$$

Author Proof

SPI Journal: 11734 MS: 0225 ☐ TYPESET ☐ DISK ☐ LE ☐ CP Disp.:2021/7/19 Pages: 14 Layout: EPJST

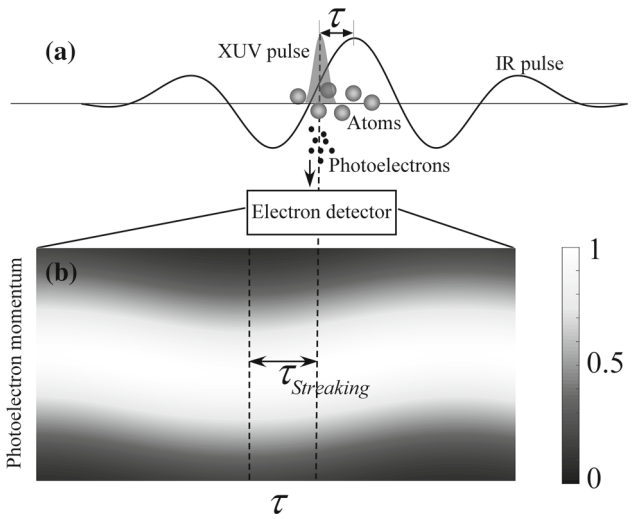

Fig. 5 Schematic diagram of attosecond streaking technique (described in the text)

where $\mathbf{p}_{\text{initial}}$ is the initial momentum of the photoelectron, and $\mathbf{A}_{\text{IR}}$ is the magnetic vector potential of the IR pulse (atomic units are used) [63]. A streaking spectrogram, the photoelectron momentum distribution with respect to XUV–IR delay τ, is shown in Fig. 5b. Analysing the spectrogram, one can get the streaking delay denoted as $\tau_{\text{Streaking}}$ in Eq. (33). $\tau_{\text{Streaking}}$ is the shift of the extremum of the photoelectron yield (centroid) along the delay axis with respect to the arrival time of the XUV pulse (position of the maximum), as shown in Fig. 5b.

For short-range potentials, $\tau_{\text{Streaking}}$ is found to be same as $\tau_{\text{EWS}}^{\text{photoionization}}$, Eq. (31) [63]. On the other hand, for the long-range potential, the logarithmic Coulomb term contributes to the time delay and the streaking time delay can be written as

$$\tau_{\text{Streaking}} = \tau_{\text{EWS}}^{\text{photoionization}} + \tau_{\text{CLC}} = \tau_{\text{EWS}}^{\text{SR+C}} + \tau_{\text{CLC}}, \tag{34}$$

where $\tau_{\text{EWS}}^{\text{SR+C}} = \hbar \frac{\partial \delta_l^{\text{SR+C}}(E)}{\partial E}$ is the EWS part of the photoionization time delay $\tau_{\text{EWS}}^{\text{photoionization}}$ and τ_{CLC} is the time shift due to the motion of electron in residual Coulomb along with the laser field (CLC: Coulomb Laser Coupling). The EWS time delay comes from the phase accumulated by the photoelectron due to its interaction with the residual system (ion/atom). For photoionization of a neutral atom, the potential between the residual ion and the photoelectron is Coulombic even at a large distance, while it is dominated by inter-electronic interactions in the small r region. The asymptotic phase shift due to the scattering by a pure Coulomb potential is

$$\delta_{l,\text{Coulomb}}(E,r) = \delta_l^C(E) + \frac{Z}{k} ln(2kr), \tag{35}$$

where $\delta_l^C(E) = \arg\Gamma\left(1 + l - i\frac{Z}{k}\right)$ is the *Coulomb phaseshift*. The total time delay due the half-scattering, i.e., the EWS time delay in single photoionization from single-electron atom, is

$$\tau_{l,\text{Coulomb}}(E,r) = \hbar \frac{\partial \delta_{l,\text{Coulomb}}(E,r)}{\partial E} = \hbar \left[\frac{\partial \delta_l^C(E)}{\partial E} + \frac{Z}{(2E)^{3/2}} \{1 - ln(2kr)\} \right]. \tag{36}$$

$\hbar \frac{\partial \delta_l^C(E)}{\partial E}$ is the part of the time delay attributed to the Coulomb phaseshift. In the case of a Coulomb potential, the term $\hbar \frac{Z}{(2E)^{3/2}} \{1 - ln(2kr)\}$ also contributes to the time delay.

For single photoionization of a many-electron atom, the EWS delay has contributions from the pure Coulomb (corresponding to the phase δ_l^C) and a short-range part of the potential due to the correlated many-body interactions of a multi-electron system (corresponding to the phase δ^{SR}). Therefore, one can write

$$\tau_{\text{EWS}}^{\text{SR+C}} = \hbar \frac{\partial \delta_l^{\text{SR+C}}(E)}{\partial E}, \tag{37a}$$

with

$$\delta_l^{\text{SR+C}}(E) = \delta_l^{\text{SR}}(E) + \delta_l^{\text{C}}(E) = \delta_l^{\text{SR}}(E) + \arg\Gamma\left(1 + l - i\frac{Z}{k}\right). \tag{37b}$$

For an appropriate description of the electronic motion, many-body correlations have to be taken into account. In that case, an additional phase appears along with the single particle phase (HF phase) to give total short-range phase δ^{SR}. However, it must be pointed out that there is no way to physically separate these two contributions to the short-range phase.

A remarkably simple and accurate expression for the measurement contribution of the time delay for the streaking experiments is given by [63]

$$\tau_{\text{CLC}}(Z,E,\omega_{\text{IR}}) = \frac{Z}{(2E)^{3/2}} \left[2 - ln(ET_{\text{IR}})\right], \tag{38}$$

where E is the kinetic energy of the photoelectron, Z is the charge of the ion, and T_{IR} is the time period of the infrared laser field. Together with the pump-probe experimental measurement of the delay, τ_{atomic}, which is $\tau_{\text{Streaking}}$ here, and an estimate of CLC time delay, one can get the EWS time delay from Eq. (34). However, it should be remembered that the expression does not take into account electron correlations and the CLC time delay does not follow such a simple form near the threshold.

Another well-established technique for measuring the EWS time delay is RABBITT, Reconstruction of Attosecond Beating by Interference of Two photon

Author Proof

SPI Journal: 11734 MS: 0225 ☐ TYPESET ☐ DISK ☐ LE ☐ CP Disp.:2021/7/19 Pages: 14 Layout: EPJST

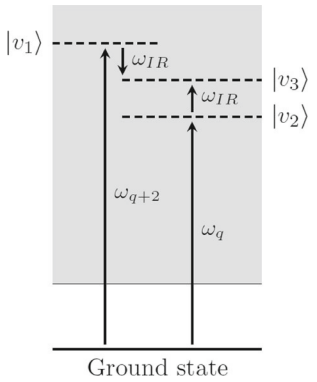

Fig. 6 Two possible paths for the final continuum state arising from a two-photon transition

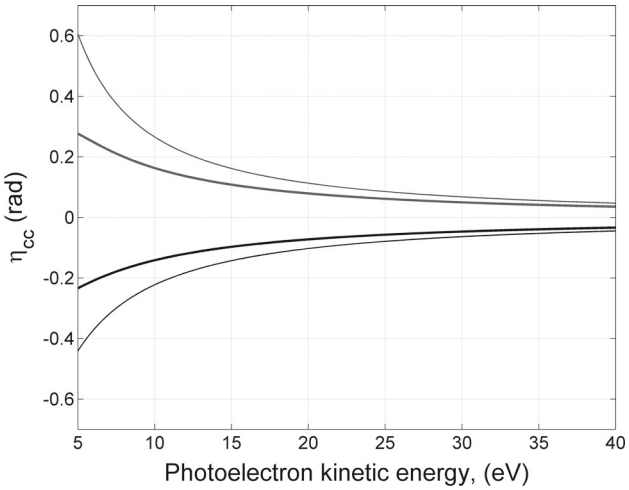

Fig. 7 Phase of the continuum–continuum transition, η_{cc}, thick curves evaluated from Eq. (40), ti.e. with the long-range amplitude correction; thin curves represent the phases corresponding the first part of Eq. (40), ti.e. without the long-range amplitude correction. Top two curves correspond to 2nd photon absorption and bottom two curves correspond to the 2nd photon emission

Transitions. In this method, instead of a single attosecond XUV pulse, an attosecond pulse train (APT) is used to ionize the system and a very weak IR field is used as a probe. The dependence of the sideband intensity with the interfering two-photon absorption and stimulated emission pathways are exploited to reveal the phase information of the atomic transitions and thus provide information about the time delay. As seen in Fig. 6, the two paths can interfere and the sideband intensity (probability of electron state $|v_3\rangle$) can be written as [3,68]

$$I_{\rm SB}(\tau) \propto cos\left(2\omega_{\rm IR}\tau + \delta\phi + \delta\phi_{\rm atomic}\right), \qquad (39)$$

where $\delta\phi$ is the difference in phase of the two consecutive harmonics in APT spectrum, and $\delta\phi_{\rm atomic}$ is the relative phase of the two transition matrix elements involved in the process. τ and $\omega_{\rm IR}$ are the controlled delay between the APT and the IR field, and the frequency of the IR field, respectively. From this relation, it is apparent that if we know the phase profile of the APT, this technique can be used to measure the atomic transition phase shift. This technique was used by Klünder *et al.* [3] to measure the relative time delay between $3s$ and $3p$ subshell photoemission from the argon atom.

In the case of any pump-probe experiment involving above-threshold ionization (ATI), as discussed earlier, there are two photon transitions. The timing information of the first photon-absorption process is obtained by the application of a second photon which serves as a clock. For the photoionization of an atom, just like the CLC time delay, there is an additional time delay $\tau_{\rm cc}$ (as mentioned in Eq. (32)) (cc: continuum–continuum) which is due to the phase accumulated in the continuum–continuum transition stimulated by the second photon. This phase shift for the hydrogenic model is given (in atomic units) by [68]

$$\eta_{\rm cc}(k_1,k_2) = \arg\left[\frac{(2k_1)^{iZ/k_1}}{(2k_2)^{iZ/k_2}}\frac{\Gamma[2+iZ(1/k_1-1/k_2)]}{(k_1-k_2)^{iZ(1/k_1-1/k_2)}}\right] + \arg\left[1+\frac{iZ}{2}(1/k_1^2+1/k_2^2)\frac{k_1-k_2}{1+iZ(1/k_1-1/k_2)}\right]. \qquad (40)$$

k_1 and k_2 stand for the photoelectron momentum, respectively, with a single-photon (pump) absorption and two-photon (pump and probe) absorption from an initial bound state. Plots of the cc phases for the second-photon emission and for the second-photon absorption for the photoionization of hydrogen atom in the ground state are shown in Fig. 7 with $\hbar\omega_{\rm IR} = 1.55\ eV$, following the work of [68]. Corresponding cc delays are shown in Fig. 8. Thick and thin curves represent the phase/delay with and without the long-range amplitude correction respectively [68]. A more accurate estimate of the cc time delay is made in [69] where many-body correlations are included.

Along with the RABBITT measurement and the estimated cc delay, one can evaluate the EWS time delay, similar to the attosecond streaking as discussed above. These attosecond pump-probe experiments have opened up a new domain in which information which was time integrated in earlier measurement schemes can now be captured [7,70–74]. One has to further consider the effect of the chirp of the ionizing XUV in the pump-probe type experiments. This causes an additional time delay which has to be taken into account for the analysis of data and retrieval of the EWS delay [75,76].

In RABBITT, one measures the delays on a discrete energy grid which is separated by $2\omega_{IR}$, whereas in streaking, one retrieves the delays on an arbitrarily spaced energy grid. This suggests the suitability of the latter method for studying narrow resonances where the former method might washout the detail. The other major difference is the effect due to the chirp of the XUV pulse; it is less important in RABBITT, but has a major contribution in streaking measurement [75]. One has to take into account of the important many-body correlation and relativistic effects to get accurate

Author Proof

SPI Journal: 11734 MS: 0225 ☐ TYPESET ☐ DISK ☐ LE ☐ CP Disp.:2021/7/19 Pages: 14 Layout: EPJST

Author Proof

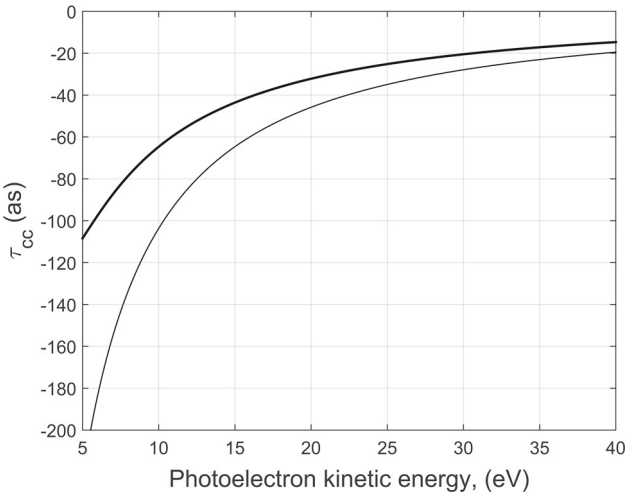

Fig. 8 Time delay in continuum–continuum transition, τ_{cc}, evaluated from the ratio of the difference between the phases of second-photon emission and second-photon absorption to the $2\hbar\omega_{IR}$. Thick and thin curves correspond to the cc delays with and without the long-range amplitude correction

value of EWS time delay, especially in the region of resonances and thresholds [49,77]. Very good agreement between the theoretical calculation of absolute EWS time delay for $3p$ subshell transition of Ar using TDLDA method and measured data using HHG plus RABBITT [78] has been reported [79].

A recent theoretical study [80] has demonstrated the RABBITT measurement with one of the harmonics below the ionization threshold, reaching the sideband above threshold through the subsequent IR absorption, whereas the other contributing harmonic to the same sideband lies in the continuum and involves continuum–continuum transition through the IR photon emission. The study of this under-threshold RABBITT (uRABBITT as it has been called) has revealed a sudden jump in RABBITT phase as a signature of the transition through a discrete bound state.

Measurement of angle resolved relative phase between two ionization pathways, one due to absorption of a single photon of frequency 2ω and the other one due to absorption of two photons of frequency ω, has been reported [81] using a new method [82]. The possibility of accessing the relative phase using bichromatic circularly polarized light has also been reported [83].

3 Recent studies on photoemission time delay from atoms, molecules, and solid surfaces

In this section, we present brief illustrations of various examples of photoionization time delay from atoms, molecules, and solid surfaces, based on the theoretical and experimental studies reported recently. Time delay has been found to depend on the angle of photoelectron ejection direction with respect to the polarization of the ionizing photon [46,52,54,84]. Significant variation of time delay with energy and angle near Cooper minima [41,42,85], around Fano resonances [43–46,86], due to giant resonances [47,48] and owing to confinement [49,50], all bear the strong signature of important electron correlations in the respective situations. In addition, a recent study [87] employed TDLDA (time-dependent local density approximation) to look into the variation of phase and time delay across Cooper minima and broad giant resonances for photoionization from noble gas and halogen atoms. Time delay from the $3d$ and $4s$ subshells of Mn get enhanced significantly due to the presence of $3p \rightarrow 3d$ giant resonance [50]. Figure 9 shows the results for the phase and time delay corresponding to the ionization from $3d$ subshell. Inclusion of the weaker channel, ti.e., $3d \rightarrow p$, in the interchannel coupling is important to understand the $3d$ time delay. 4 s photoemission time delay has been found to be very sensitive to correlations in the final ionic core state left after the photoelectron escapes from the field of the residual ion. The inclusion of escape channels that are normally considered to be weak has also been found to be important. Time delay corresponding to $4s\uparrow$ and $4s\downarrow$ turn out to be quite different in the $3p \rightarrow 3d$ giant resonance region [47].

Time delay [46] across autoionization resonances have been found to be strongly angle-dependent as seen in Fig. 10. Interchannel coupling between weak and strong photoionization channels and their out-of-phase behaviour were found to be responsible for this dramatic variation. Angle-dependent time delay profiles also revealed important relativistic effects even for the rather low-Z Ne atom. Spin-resolved time delay measurement is a reality [88,89] at the present time. A recent study [90] on Xe $4d$ photoionization has reported significantly different time delays associated with two different ionization mechanisms involved in the process. Significant impact of many-body correlation effects due to interchannel coupling [91,92], or spin-orbit interaction activated interchannel coupling (SOIAIC) [51,52,93] has been also observed in photoionization time delay.

Studies of photodetachment [37,38,92] are of particular importance, since the ejected photoelectron does not move in the field of a Coulomb potential, unlike the case of photoionization and, hence, the time results is not contaminated by this additional long-range Coulomb interaction. This results in a negligible value of cc delay with respect to the EWS delay in high photoelectron energy regime; but, as one goes very near the threshold, i.e., the low photoelectron energy, cc delay starts deviating from the near zero value even for these negative ions [37]. Photodetachment time delay for Cl^- $3p$ shows a sharp decrease just above the photodetachment threshold, followed by a rise, as depicted in Fig. 11 [38]. This is partially a consequence of the d-wave shape resonance that affects the photodetachment time delay strongly; in the photoionization of the isoelectronic neutral system, ti.e., Ar, the Coulomb field eclipses this effect.

SPI Journal: 11734 MS: 0225 ☐ TYPESET ☐ DISK ☐ LE ☐ CP Disp.:2021/7/19 Pages: 14 Layout: EPJST

Author Proof

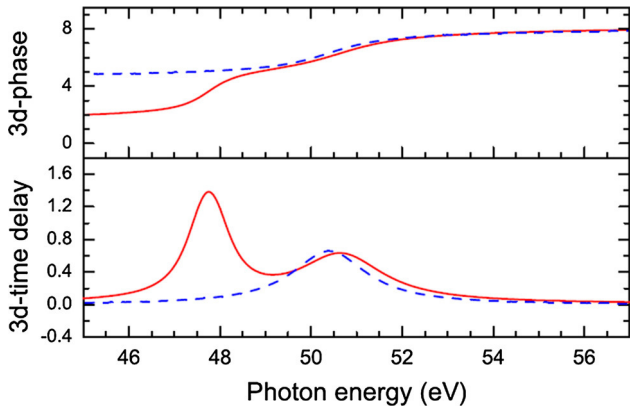

Fig. 9 Phase and time delay for Mn $3d$ photoionization showing the enhancement due to the presence of $3p \rightarrow 3d$ giant resonance [47]. (Solid curve) coupled-channel calculation; (dashed curve) single-channel calculation

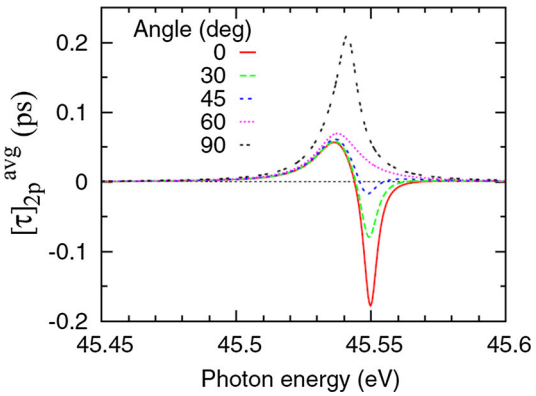

Fig. 10 Photoionization time delay from the $2p_{1/2}$ subshell of Ne around $2s \rightarrow 3p$ autoionization resonance. Different colours indicate time delay profile for different angles [46]

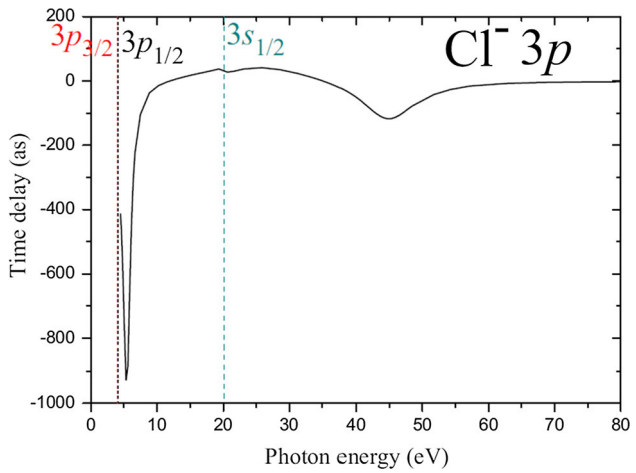

Fig. 11 Photodetachment time delay from the $3p$ subshell of Cl^- [38]. Vertical lines show the respective thresholds

Now, the studies on molecular photoionization are very different as they do not possess central field symmetry, unlike the atomic scenario. The difficulties in examining molecular systems [94] are mainly due to the following facts: a) the initial bound state is composed of a large number of partial waves having different angular momenta, complicating the situation even more while ionizing to a host of accessible final states, and b) the orientation of the molecule is an important factor to consider.

Studies on photoionization time delay from N_2 and CO have revealed [95] a significant angle dependence, the signature of shape resonance of N_2, and asymmetric time delay for CO along with the indication of the repulsive field near the electronegative oxygen atom causing a time advancement rather than delay, ti.e., negative time delay. The time delay results for N_2O and H_2O molecules [94,96] indicate a monotonic profile for H_2O, whereas the presence of a shape resonance is reflected for N_2O. Additional structures are observed in the two-photon consideration with a substantial shift of the peak in time delay occurring due to shape resonance in the orientation-averaged calculation. Studies on stereo Wigner time delay (SWTD) on CO molecules, based on the photoelectron ejection from different sites of the molecule, show significant values [97] and suggest preferential ejection of photoelectron as well from different states for dissociative ionization [98]. The results of an SWTD calculation, shown in Fig. 12, suggested that the photoelectron is likely to be ejected from the carbon site at lower energies corresponding to Σ states, showing large negative time delay. The preferential ejection site shifts to the oxygen end for higher energies in the parallel orientation of the molecule, showing a shift toward positive time delay. The Π states correspond to the perpendicular orientation of the molecule and show positive time delay.

It has been demonstrated in a recent work [99] that the birth of the photoelectron wave from two centres of H_2 does not occur simultaneously. There is a time delay of 247 zeptoseconds (10^{-21} s) involved, as shown in Fig. 13, due to the travel time of photon across the bond length. This has been measured by observing a shift in the interference pattern, since a phase difference is involved between the photoelectron waves corresponding to the electrons launched from two sides of H_2 molecule.

Another study [100] has reported an excess time delay of 50 to 70 as for photoemission from liquid water compared to isolated gaseous water molecule. This extra delay has been attributed to the local environment in the liquid phase with a number of solvation shells around. The contribution to the delay from the transport of the photoelectron in this environment is found to be negligible.

Smith [101] discussed the connection between the collision lifetime and the quasi-equilibrium constant for association/dissociation in case of atom–atom recombination, which was subsequently generalized for atom–molecule and molecule–molecule scattering by Bowman [102], using the idea of density of resonance states. Due to the connection between the collision lifetime and the resonance lifetime for Feshbach resonances, the trace of

SPI Journal: 11734 MS: 0225 ☐ TYPESET ☐ DISK ☐ LE ☐ CP Disp.:2021/7/19 Pages: 14 Layout: EPJST

Author Proof

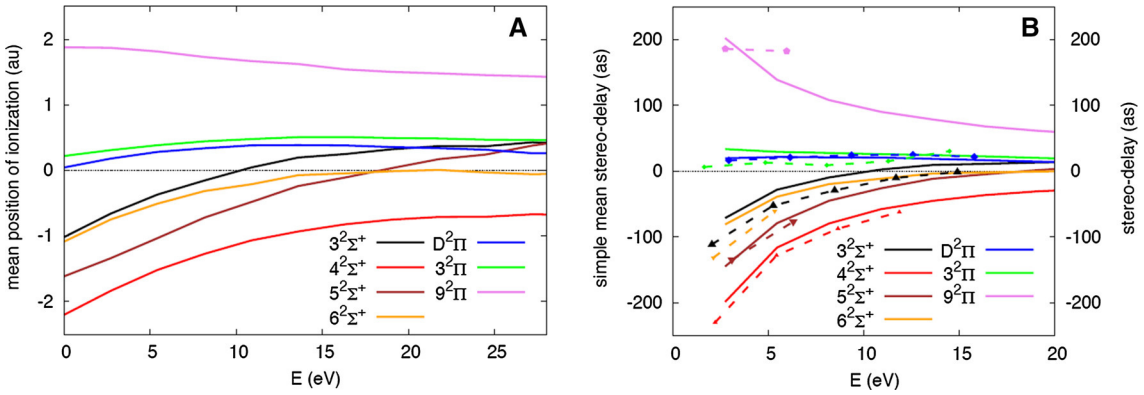

Fig. 12 Photoionization of CO. **a** Mean position of the birthplace of the photoelectron at different energies; different colours indicate different molecular states. **b** Time delay from different molecular states over a range of energies. Both the figures are for the case when the molecule is oriented in parallel to the field [98]

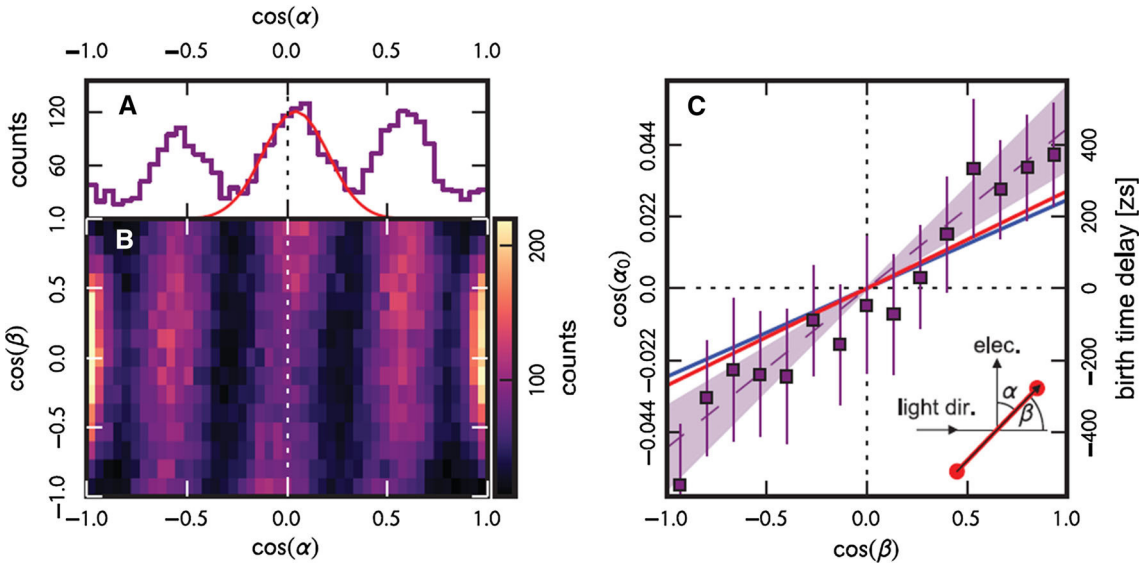

Fig. 13 **a** Inference pattern due to the photoelectron wavepackets emerging from two atomic sites of a diatomic molecule. **b**, **c** Exhibit a substantial shift of the fringe pattern based on the direction of the light field that influences the motion of the electron from one site to the other causing a time delay of 247 *zs*. β represents the orientation of the molecule with respect to the polarization of the ionizing field and α is the shift of the interference fringe from the mean position [99]

the collision lifetime matrix has been considered for a few cases to get information about the resonant states [103]. Electromagnetic field-induced geometric phase is known to affect the time delay significantly [104]. Time delay profiles in the region of resonances occurring at different energy regimes for ultracold atomic and molecular collisions have also been examined recently [105].

There are quite a few extant studies investigating the EWS time delay from nanostructures like fullerenes and atoms inside fullerenes. The cage is mimicked with different model potentials and different approaches are in business to examine these nanostructures. Time-dependent local density approximation (TDLDA) studies on Ar@C_{60} have revealed the nature of time delay being negative and positive, respectively, due to the $3p-$bonding and antibonding states [49], the effect of giant plasmon resonance [106], and cavity minima [77].

Oscillations in time delay due to confinement resonances have been reported for He+@C_{60} [107] and Xe@C_{60} [50]. Photoionization studies for Xe $4d$ encaged in C_{60} [50] have shown that although confinement oscillations are present in cross section, they get suppressed in the dipole photoionization angular distribution, since it is a ratio. The oscillations, however, are much more prominent in the time delay which, therefore, emerges as a more sensitive indicator of confinement dynamics. Being the energy derivative of the phase, time delay carries a sensitive signature of confinement, as shown in Fig. 14. The same phenomena for photoionization of the $1s$ of H@C_{60}, $3p$ of Ar@C_{60}, and $5p$ of Xe@C_{60} were observed in a recent study [108] using

SPI Journal: 11734 MS: 0225 ☐ TYPESET ☐ DISK ☐ LE ☐ CP Disp.:2021/7/19 Pages: 14 Layout: EPJST

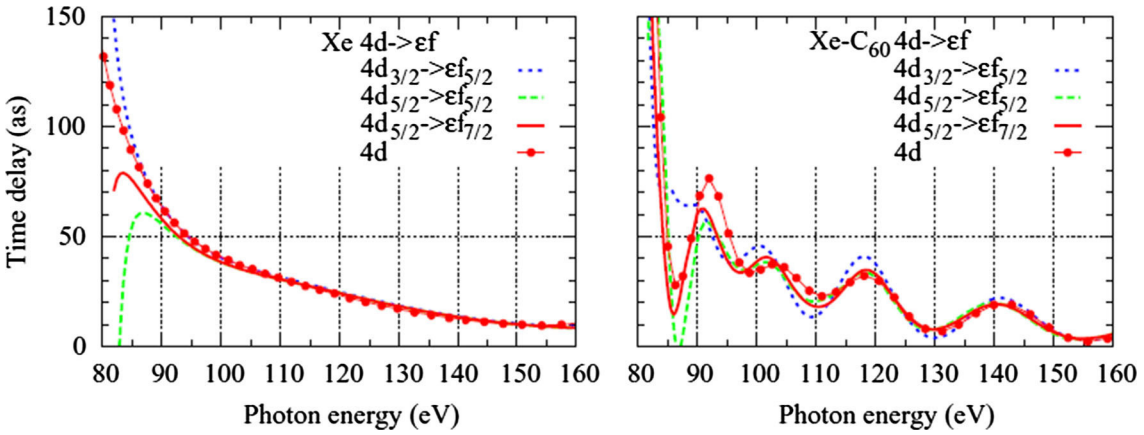

Fig. 14 Time delay corresponding to different ionizing channels from $4d$ subshell of free and confined xenon, Xe and Xe@C_{60}. Oscillations in the case of encaged atom due to confinement resonances [50] are seen

the transient phase method with the single-active electron (SAE) approximation. The effects of Coulomb confinement resonances on inner and outer shell photoionization, along with the dependence on charge residing on the cage, have been studied for endohedral anions [109]. The effects of dipole static polarization (DSP) and interior static polarization (ISP) of the fullerene cage have been addressed [110], along with the varying impact of the size of the C_N cage in another study [111]. The effects of polarization of the cage by the IR probe tends to get cancelled by the screening of the IR probe; the screening of the IR field by the cage would cause a time delay of ~ 100 as, whereas the polarization of the cage by the same IR probe creates strong dipole-laser coupling that causes time advancement by about the same amount. An angle-dependent study on $4d$ photoionization from Xe@C_{60} revealed [51] the presence of Cooper-like minima and relativistic effects. And the scattering of electrons by a fullerene cage and the time delay in the process have also been studied [112] using the Dirac bubble potential model.

Recently, the scattering phase and EWS time delay for elastic scattering of slow electrons by small molecules have been computed within the frame of a non-overlapping atomic potentials model [113,114]. Attosecond time-resolution along with high spectral resolution enabled experimentalists to temporally resolve the effects of motion of nucleus on the electron emission from the molecular shape resonance region beyond the usual Franck–Condon approximation [115]. The angle and energy dependence of the EWS time delay was studied for partial two-center spheroidal Coulomb waves. The role of the Cooper minimum leading to singularities in EWS time delay was also investigated [116]. Multi-electron correlation effects on photoionization time delays were studied using a variant of RABBITT in combination with many-body calculations [117]. Measurement of CLC time delay was performed using a reaction microscope at the THz beamline of the free-electron laser in Hamburg (FLASH) [118], which is necessary to disentangle CLC and EWS time delay contributions in attosecond streaking measurements. The nature of time delay across autoionization resonances and its connection with the resonance lifetime has also been pointed out [85]. Studies on time delay measurements have also been extended toward photoemission from solid surfaces. Electrons from the localized $4f$ states are observed to emerge with an average delay of 100 as compared to the ones originating from the delocalized conduction band [1]. Considerations of smaller mean velocity and longer inelastic mean free paths for the $4f$ electrons, within a quantum mechanical treatment, were identified as the cause of 90 as of the delay, which was pretty close to the experimental values. Interestingly, a similar study on the electrons from the valence and core of single crystalline magnesium shows no relative delay [7]. Time delay studies on solids [119–128] have reported the effects of several important factors like band structure, electron transport, IR skin depth of the material, penetration through the surface barriers, *etc.*

Summary and conclusions

Eisenbud–Wigner–Smith time delay formalism is discussed in the context of time-reversal symmetry between collision and photoionization/photodetachment. Time delay is identified as an observable represented by a self-adjoint operator notwithstanding the fact that there is no such operator for time itself. Attosecond streaking and RABBITT techniques to determine EWS time delay are discussed. A few illustrative examples of theoretical and experimental studies of time delay from the very vast and rapidly extending literature are mentioned.

Time delay has been found to depend on the angle of photoelectron ejection direction with respect to the polarization of the ionizing photon. Significant variation of time delay with energy and angle are found near Copper minima, across autoionization resonances, giant resonances, and owing to confinement. Angle-dependent time delay profiles have revealed important

Author Proof

SPI Journal: 11734 MS: 0225 ☐ TYPESET ☐ DISK ☐ LE ☐ CP Disp.:2021/7/19 Pages: 14 Layout: EPJST

relativistic effects even for rather low-Z Ne atom. Significant impacts of many-body correlation effects due to interchannel coupling, or spin-orbit interaction activated interchannel coupling (SOIAIC) have been also observed in photoionization time delay. Sharp structure in EWS time delay in photodetachment is found which is eclipsed in photoionization of neutral atom due to the presence of Coulomb field in the later case. Significant angle dependence of EWS time delay is found in photoionization of molecules. It is realized that the EWS time delay could be a very sensitive probe to study encaged systems/nanostructures, molecular environment for the liquid-phase photoionization to electron dynamics in solid-state materials. However, there are a few open problems in atom–laser interaction [63] which have to be addressed in the future.

Acknowledgements We are thankful to Professor J. M. Dahlström (Lund University) for very helpful discussions on the cc delay. The work of STM was supported by the U.S. Department of Energy, Office of Science, Basic Energy Sciences, under Award # DE-FG02-03ER15428.

Author contribution statement

PCD: project supervision, project administration, and validation of analysis and manuscript refinement and edits. SB: computation, investigation, analysis, methodology, data curation, and manuscript preparation. AM: computation, investigation, analysis, methodology, data curation, and manuscript preparation. STM: project supervision, project administration, and validation of analysis and manuscript refinement and edits.

References

1. A.L. Cavalieri et al., Nature **449**, 1029 (2007)
2. M. Schultze et al., Science **328**, 1658 (2010)
3. K. Klünder et al., Phys. Rev. Lett. **106**, 143002 (2011)
4. L. Eisenbud, Ph. D. thesis, Princeton University (1948)
5. E.P. Wigner, Phys. Rev. **98**, 145 (1955)
6. F.T. Smith, Phys. Rev. **118**, 349 (1960)
7. S. Neppl et al., Phys. Rev. Lett. **109**, 087401 (2012)
8. M. Drescher et al., Nature **419**, 803 (2002)
9. H.M. Nussenzveig, Phys. Rev. D **6**, 1534 (1972)
10. P.A. Martin, *New Developments in Mathematical Physics* (Springer, Vienna, 1981), pp. 157–208
11. K. Gustafson, K. Sinha, Lett. Math. Phys. **4**, 381 (1980)
12. A. Jensen, Commun. Math. Phys. **82**, 435 (1981)
13. M. Bauer, P.A. Mello, K.W. McVoy, Z. Phys. A **293**, 151 (1979)
14. C. Maroni, I. Massa, G. Vannini, Phys. Lett. B **60**, 344 (1976)
15. E. Doron, U. Smilansky, A. Frenkel, Phys. Rev. Lett. **65**, 3072 (1990)
16. E.P. Kanter et al., Phys. Rev. Lett. **35**, 1326 (1975)
17. J.P. Svenne et al., Phys. Rev. C **40**, 1136 (1989)
18. N.G. Kelkar, M. Nowakowski, K.P. Khemchandani, J. Phys. G **29**, 1001 (2003)
19. Nucl. Phys. A **724**, 357 (2003)
20. Nucl. Phys. A **730**, 121 (2004)
21. E.E. Kolomeitsev, D.N. Voskresensky, J. Phys. G **40**, 113101 (2013)
22. P. Ambichl et al., Phys. Rev. Lett. **119**, 033903 (2017)
23. J. Carpenter, B.J. Eggleton, J. Schröder, Nat. Photon. **9**, 751 (2015)
24. Y.V. Fyodorov, H.J. Sommers, J. Math. Phys. **38**, 1918 (1997)
25. C. Texier, Physica E **82**, 16 (2016)
26. C.A. de Carvalho, H.M. Nussenzveig, Phys. Rep. **364**, 83 (2002)
27. P.C. Deshmukh, S. Banerjee, Int. Rev. Phys. Chem. **40**, 127 (2021)
28. T.Y. Wu, T. Ohmura, *Quantum Theory of Scattering* (Courier Corporation, Chelmsford, MA, 2014)
29. G. Muga, R. S. Mayato, I. Egusquiza (Eds.), Time in Quantum Mechanics (Springer, Berlin, 2007), Vol. 734
30. J.M. Jauch, K.B. Sinha, B.N. Misra, Helv. Physica Acta **45**, 398 (1972)
31. W.O. Amrein, *Hilbert Space Methods in Quantum Mechanics* (EPFL Press, Lausanne, 2009)
32. M. Bruni, S. Sonego, Class. Quant. Gravity **16**, L29 (1999)
33. M.J. Hu, X.M. Hu, Y.S. Zhang, Quant. Stud.: Math. Found. **4**, 243 (2017)
34. U. Fano, A. R. P. Rau, Atomic Collisions and Spectra (Elsevier, Amsterdam, 2012)
35. P.C. Deshmukh, D. Angom, A. Banik, *Symmetry in Electron–Atom Collision and Photoionization Process* (DST-SERC-School publication, Narosa, 2011)
36. O. C. de Beauregard, CPT Revisited: A Manifestly Covariant Presentation. In *The Wave-Particle Dualism* (Springer, Dordrecht, 1984), pp. 485–497
37. E. Lindroth, J.M. Dahlström, Phys. Rev. A **96**, 013420 (2017)
38. S. Saha et al., Phys. Rev. A **99**, 043407 (2019)
39. A.S. Kheifets, Phys. Rev. A **87**, 063404 (2013)
40. S. Saha et al., Phys. Rev. A **90**, 053406 (2014)
41. D. Hammerland et al., arXiv:1907.01219 (2019)
42. A.S. Kheifets, D. Toffoli, P. Decleva, J. Phys. B **53**, 115201 (2020)
43. M. Sabbar et al., Phys. Rev. Lett. **115**, 133001 (2015)
44. V. Gruson et al., Science **354**, 734 (2016)
45. C. Cirelli et al., Nat. Commun. **9**, 1 (2018)
46. S. Banerjee et al., Phys. Rev. A **99**, 013416 (2019)
47. V.K. Dolmatov et al., Phys. Rev. A **91**, 053415 (2015)
48. M. Magrakvelidze, M.E.A. Madjet, H.S. Chakraborty, Phys. Rev. A **94**, 013429 (2016)
49. G. Dixit, H.S. Chakraborty, M.E.A. Madjet, Phys. Rev. Lett. **111**, 203003 (2013)
50. P.C. Deshmukh et al., Phys. Rev. A **89**, 053424 (2014)
51. D.A. Keating, P.C. Deshmukh, S.T. Manson, J. Phys. B **50**, 175001 (2017)
52. A. Mandal et al., Phys. Rev. A **96**, 053407 (2017)
53. A.W. Bray, F. Naseem, A.S. Kheifets, Phys. Rev. A **98**, 043427 (2018)
54. J. Wätzel et al., J. Phys. B **48**, 025602 (2014)
55. W.R. Johnson, C.D. Lin, Phys. Rev. A **20**, 964 (1979)
56. Phys. Rev. A **14**, 565 (1976)

Author Proof

Author Proof

57. A. Dalgarno, G.A. Victor, Proc. Roy. Soc. Ser. A. Math. Phys. Sci. **291**, 291 (1966)
58. M.Y. Amusia, N.A. Cherepkov, Case Stud. Atom. Phys. **5**, 47 (1975)
59. D. Strickland, G. Mourou, Opt. Commun. **55**, 447 (1985)
60. P.B. Corkum, Phys. Rev. Lett. **71**, 1994 (1993)
61. M. Lewenstein et al., Phys. Rev. A **49**, 2117 (1994)
62. R. Kienberger et al., Nature **427**, 817 (2004)
63. R. Pazourek, S. Nagele, J. Burgdorfer, Rev. Mod. Phys. **87**, 765 (2015)
64. L. Gallmann, C. Cirelli, U. Keller, Ann. Rev. Phys. Chem. **63**, 447 (2012)
65. C. Palatchi et al., J. Phys. B **47**, 245003 (2014)
66. I.A. Ivanov, A.S. Kheifets, V.V. Serov, Phys. Rev. A **86**, 063422 (2012)
67. R. Pazourek, S. Nagele, J. Burgdorfer, Faraday Discus. **163**, 353–376 (2013)
68. J.M. Dahlström et al., Chem. Phys. **414**, 53 (2013)
69. J.M. Dahlström et al., Phys. Rev. A **86**, 061402 (2012)
70. F. Krausz, M. Ivanov, Rev. Mod. Phys. **81**, 163 (2009)
71. D. Guenot et al., Phys. Rev. A **85**, 053424 (2012)
72. V.S. Yakovlev et al., Phys. Rev. Lett. **105**, 073001 (2010)
73. A.S. Kheifets, I.A. Ivanov, Phys. Rev. Lett. **105**, 233002 (2010)
74. L.R. Moore et al., Phys. Rev. A **84**, 061404 (2011)
75. L. Cattaneo et al., Opt. Express **24**, 29060 (2016)
76. L. Seiffert et al., Nat. Phys. **13**, 766 (2017)
77. M. Magrakvelidze et al., Phys. Rev. A **91**, 053407 (2015)
78. S.B. Schoun et al., Phys. Rev. Lett. **112**, 153001 (2014)
79. M. Magrakvelidze et al., Phys. Rev. A **91**, 063415 (2015)
80. A.S. Kheifets, A.W. Bray, Phys. Rev. A **103**, L011101 (2021)
81. D. You et al., Phys. Rev. X **10**, 031070 (2020)
82. Di. Fraia et al., Phys. Rev. Lett. **123**, 213904 (2019)
83. S. Donsa et al., Phys. Rev. Lett. **123**, 133203 (2019)
84. A.S. Kheifets et al., Phys. Rev. A **94**, 013423 (2016)
85. M. Nisoli, G. Sansone, Prog. Quant. Electron. **33**, 17 (2009)
86. P.C. Deshmukh et al., J. Phys. B **51**, 065008 (2018)
87. L.W. Pi, A.S. Landsman, Appl. Sci. **8**, 322 (2018)
88. M. Fanciulli et al., Phys. Rev. Lett. **118**, 067402 (2017)
89. M. Fanciulli, SciPost Phys. **5**, 058 (2018)
90. S. Zhong et al., Nat. Comm. **11**, 5042 (2020)
91. D.A. Keating et al., Phys. Rev. A **98**, 013420 (2018)
92. S. Saha et al., Phys. Rev. A **99**, 063413 (2019)
93. S. Banerjee et al., Phys. Rev. A **101**, 043411 (2020)
94. D. Baykusheva, H.J. Wörner, J. Chem. Phys. **146**, 124306 (2017)
95. P. Hockett et al., J. Phys. B **49**, 095602 (2016)
96. M. Huppert et al., Phys. Rev. Lett. **117**, 093001 (2016)
97. A. Chacon, M. Lein, C. Ruiz, Phys. Rev. A **89**, 053427 (2014)
98. J.L. Vos et al., Science **360**, 1326 (2018)
99. S. Grundmann et al., Science **370**, 339 (2020)
100. I. Jordan et al., Science **369**, 974 (2020)
101. F. T. Smith, in Kinetic Processes in Gases and Plasmas, edited by A. R. Hochstim (Academic: New York, 1969)
102. J.M. Bowman, J. Chem. Phys. **90**, 3492 (1986)
103. B. Kendrick, R.T. Pack, Chem. Phys. Lett. **235**, 291 (1995)
104. B. Kendrick, R.T. Pack, J. Chem. Phys. **104**, 7502 (1996)
105. M.D. Frye, J.M. Hutson, Phys. Rev. Res. **1**, 033023 (2019)
106. T. Barillot et al., Phys. Rev. A **91**, 033413 (2015)
107. S. Nagele et al., J. Phys.: Conf. Ser. **488**, 012004 (2014)
108. S. Saha et al., Eur. Phys. J. Plus **135**, 753 (2020)
109. A. Kumar et al., Phys. Rev. A **94**, 043401 (2016)
110. V. K. Dolmatov, arXiv:1809.02898 (2018)
111. V.K. Dolmatov, A. Edwards, J. Phys. B **52**, 105001 (2019)
112. M.Y. Amusia, A.S. Baltenkov, J. Phys. B **52**, 015101 (2018)
113. A.S. Baltenkov, S.T. Manson, A.Z. Msezane, J. Phys. B **51**, 205101 (2018)
114. M.Y. Amusia, A.S. Baltenkov, JETP **131**, 707 (2020)
115. S. Nandi et al., Sci. Adv. **6**, eaba7762 (2020)
116. V.V. Serov, V.L. Derbov, T.A. Sergeeva, Phys. Rev. A **87**, 063414 (2013)
117. A. Kamalov et al., Phys. Rev. A **102**, 023118 (2020)
118. G. Schmid et al., Phys. Rev. Lett. **122**, 073001 (2019)
119. C.H. Zhang, U. Thumm, Phys. Rev. Lett. **102**, 123601 (2009)
120. C. Lemell et al., Phys. Rev. A **79**, 062901 (2009)
121. A.K. Kazansky, P.M. Echenique, Phys. Rev. Lett. **102**, 177401 (2009)
122. J.C. Baggesen, L.B. Madsen, Phys. Rev. A **78**, 032903 (2008)
123. E.E. Krasovskii, Phys. Rev. B **84**, 195106 (2011)
124. A.G. Borisov et al., Phys. Rev. B **87**, 121110 (2013)
125. C.H. Zhang, U. Thumm, Phys. Rev. A **84**, 033401 (2011)
126. R.L. Locher et al., Optica **2**, 405 (2015)
127. Z. Tao et al., Science **353**, 62 (2016)
128. M. Ossiander et al., Nature **561**, 374 (2018)

SPI | Journal: **11734** MS: **0225** ☐ TYPESET ☐ DISK ☐ LE ☐ CP Disp.:**2021/7/19** Pages: **14** Layout: **EPJST**